Proceedings of ESDA2006
8th Biennial ASME Conference on Engineering Systems Design and Analysis
4-7 July, 2006, Torino, Italy

DRAFT Paper Number 95738

NUMERICAL SIMULATIONS OF REACTIVE MIXTURE FLOW IN THE ANODE LAYER OF SOLID OXIDE FUEL CELLS BY THE LATTICE BOLTZMANN METHOD

Pietro Asinari [a, *], Michele Calì Quaglia [a], Michael R. von Spakovsky [b], Bhavani V. Kasula [b]

[a] Energy Engineering Department, Politecnico di Torino
Corso Duca degli Abruzzi 24, Torino, Zip Code 10129, Italy
Emails: pietro.asinari@polito.it, michele.cali@polito.it
[*] Corresponding author. Tel. +39-011-564-4413, Fax. +39-011-564-4499.

[b] Center for Energy Systems Research, Mechanical Engineering Department
Virginia Polytechnic Institute and State University (Virginia Tech)
Blacksburg, VA 24061, U.S.A.
Emails: vonspako@vt.edu, bvkasula@vt.edu

ABSTRACT

Mathematical models that predict performance can aid in the understanding and development of solid oxide fuel cells (SOFCs). Obviously various modeling approaches exist involving different length scales. In particular, very significant advances are now taking place in understanding the complex composite structures of electrodes and three-phase boundaries. Ultimately these advances should lead to predictions of cell behavior, which at present are measured empirically and inserted into macroscopic cell models.

In order to achieve this ambitious goal, simulation tools of these macroscopic models must be redesigned by matching them to the complex microscopic phenomena, which take place at the pore scale. As a matter of fact, the macroscopic continuum approach essentially consists of applying some type of homogenization technique, which properly averages the underlying microscopic phenomena for producing measurable quantities. Unfortunately, these quantities in the porous electrodes of fuel cells are sometimes measurable only in principle. For this reason, this type of approach introduces uncertain macroscopic parameters, which can significantly affect the numerical results, particularly their generality.

This paper is part of an ongoing effort to address the problem following an alternative approach. The key idea is to numerically simulate the underlying microscopic phenomena in an effort to bring the mathematical description nearer to actual reality. In particular, some recently developed mesoscopic tools appear to be very promising since the microscopic approach is, in this particularly case, partially included in the numerical method itself. In particular, the models based on the lattice Boltzmann method (LBM) treat the problem by reproducing the collisions among particles of the same type, among particles belonging to different species, and finally among the species and the solid obstructions.

Recently, a model based on LBM for calculating the fluid flow of a reactive mixture in randomly generated porous media by simulating the actual coupling interaction among the species was proposed. A parallel three–dimensional numerical code was developed in order to implement this model and to simulate the actual microscopic structures of SOFC porous electrodes.

In this paper, a thin anode (50 micron) of Ni-metal / YSZ-electrolyte cermet for a high–temperature electrolyte supported SOFC was considered in the numerical simulations. The three–dimensional anode structure was derived by a regression analysis based on granulometry law of some microscopic pictures obtained with an electron microscope. The numerical simulations show the spatial distribution of the mass fluxes for the reactants and the products of the electrochemical reactions. The described technique should allow to design new improved materials in order to statistically optimize these fluid paths.

INTRODUCTION

The solid oxide fuel cells (SOFCs) are receiving considerable interest since they are suited for both stationary and vehicle applications [1,2,3]. The reduction of activation polarization, the elimination of expensive catalysts, potential integration with cogeneration systems and the possibility to consider syngas of different composition as fuel are interesting technical challenges. The Department of Energy (DOE) of United States has recently started a research project (SECA, Solid State Energy Conversion Alliance) with the purpose to increase the power density, to reduce the manufacturing costs and to encourage commercially cost-effective prototypes; the European Union, through the European Hydrogen and Fuel Cell Technology Platform: Strategic Research Agenda (January 2005), indicates the SOFC as a priority choice for stationary applications.

The typical solid oxide structure involves a thick electrolyte of yttria stabilized zirconia (ZrO_2 + 8% Y_2O_3) for the electrolyte supported (ES) cells. The function of the YSZ ceramic support is to maintain the stability of the electronically conductive nickel-metal particles and to provide an anode thermal expansion coefficient acceptably close to those of the electrolyte. The YSZ part of the cermet structure also serves partially as the ionic conductor. Very thin layers (50-100 μm are typical values) are coated on both sides for realizing the cathode and the anode

elements, which must be consistent with the actual operating conditions (900–1000 °C).

Recently, a new trend during recent years is to employ thick porous electrodes, which are made of cermet [4,5,6]. This practice allows to lower the operating temperature to a moderate range (700–850 °C) and consequently to reduce the material cost and the requirements for auxiliaries. Concerning the cathode electrode, a material addressing the technical requests is lanthanum manganite suitably doped with alkaline (calcium) and rare earth (strontium) elements, in order to improve its electronic conductivity ($La_{0.7}Sr_{0.3}MnO_3$). This material allows to reduce the cathode layer thickness to 1 mm in cathode supported (CS) cells and 0.1 mm in anode supported (AS) ones. Concerning the anode electrode, its basis material is a skeleton of yttria stabilized zirconia (YSZ) around Ni particles. The anode layer thickness is in the order of 0.1 mm (CS) and 1.5 mm (AS).

In many international research centers, most of investigations are focused on the experimental analysis of single cells SOFC under the typical operating conditions or on small stack fed from various fuel, like gas made up of methane or hydrogen [7]. The objective of these researches is to understand the phenomena that are to the base of the operation and the stability of the cells [8], characterizing the electrochemical behavior of single cell's components and identifying the optimal operating conditions for its operation [9,10].

The research work is based on the electrochemical characterization of a single SOFC in the typical conditions of operation. The performances are recorded according to some parameters such as fuel composition, pressure of reagents, operating temperature of the cell, eventual phenomena of macroscopic degradation (as an example de-lamination or carbon deposition [8]), cell polarization losses related to processes of microscopic degradation (evolution of the microstructure of anode [11,12,13,14,15], cathode [16,17], electrolyte [18,19,20]); sometimes these phenomena are investigated resorting to morphologic analysis of the materials before and after the phases of operation also by the use of sophisticated technologies, as an example scanning electron microscope (SEM).

These microscopic phenomena investigated in the literature refer, for example, to the electrodes. The cathode electrode can be affected by kinetic de-mixing; the phenomena doesn't seem related to the cell operating temperature but to the fact that material is affected by the electric field under a current load condition; these conditions could lead to the pore formation in the material which is major concentrated at the cathode/electrolyte interface and it could cause losses of electrochemical performances. The applied current creates an oxygen potential gradient and this difference could be the driving force for the pore formation [16]. As concerning the anode electrode, it could be affected by nickel agglomeration. It could be explained like a degradation of the three phase boundary (TPB) because of sintering of metal particles and decreasing of contact area at the electrolyte/anode interface and a decrease of the specific surface area of Ni particles [15].

The mass transport phenomena through the electrode materials represent the key issue. The thickness of the electrodes, their porosity (in volume fraction), the pore dimensions, the tortuosity factor and the pore connections are the main parameters affecting the mass transport of chemical species through the electrode/electrolyte interface [21]. The mass transport of chemical species determines has a great influence on the concentration overpotentials on anode and cathode side (in particular, the cell voltage is mainly affected by the cathode layer thickness [22, 23]), and modifies the fuel reforming rate on the electrode surface of the anode side, causing temperature non-uniformity and mechanical failure due to thermally induced stresses [24].

Because of the difficulties in realizing prototypes, an extensive simulation activity can be found in open literature [25-27]. Many models are based on the assumption that the structure of the porous medium is isotropic so that the cermet can be described by three structural parameters (the ratio of porosity to tortuosity, the mean value and the standard deviation of the pore radii). They are used to compute the phenomenological coefficients which are involved into the constitutive correlations for the diffusion and the permeation (MTPM – mean transport pore model) [28]. In particular the diffusion and the permeation phenomena depend on conventional molecular effects and on kinetic effects, since some of the pore radii are comparable to the mean free path of flowing fluids. In particular, for an anode-supported SOFC where high fuel utilization is required, a small error in the concentration overpotential calculation, which is mainly affect by mass transport inside porous anode, may cause a dramatic change to its design performance [29]. Some experiments have been performed in order to determine the structural parameters for cermet materials [30]. These experiments and additional theoretical reasons induce to consider among structural parameters that the ratio of porosity to tortuosity and the mean value of pore radii affect the reaction rate mostly [30]. However at the moment, the suitability of structural parameters and of the constitutive correlations to describe macroscopic flow rate has not been completely verified for cermet involved into SOFC. This is due to reasons:

- many different microscopic topologies are possible which share the same values for structural parameters, since they are macroscopic observable which predict averaged properties;
- there is a lot of working conditions for porous electrodes and for this reason it is very difficult to verify experimentally the constitutive correlations which describe the diffusion and the permeation in all practical ranges.

Despite the success of macroscopic modeling in understanding the complex phenomena occurring during fuel cell operation and in contributing to improved fuel cell designs, the actual micro structure of the porous layers that constitute a fuel cell is usually not modeled. Its effects on cell operation and performance are taken into account by considering homogeneous layers characterized by macroscopic, averaged parameters such as porosity and tortuosity.

While this eases the modeling efforts, it carries two disadvantages. Firstly, if an in–situ measurement of such macroscopic quantities is performed, the related uncertainties are bound to affect the model results, whereas if porosity and tortuosity are treated as fitting parameters, there is no guarantee that the true values are used since such parameters can be used to compensate for the inaccurate modeling of other phenomena. Secondly, it has been shown [31] that different porous layer micro structures, characterized by the same porosity, show different hydraulic characteristics. In other words, no macroscopic parameter can exhaustively describe what happens at microscopic levels.

In order to overcome these limitations, a novel approach to gas flow modeling in porous media, based on the lattice Boltzmann methods (LBMs), was utilized. LBMs are efficient numerical tools for investigating flow in highly complex geometries, such as porous media [32-34]. Even though traditional Navier-Stokes solvers could be used to describe porous media flow, LB methods do not require pressure-velocity decoupling or the resolution of a large system of algebraic equations [35, 36]. They solve a simplified Boltzmann equation for an ensemble-averaged distribution of moving, interacting particles on a discrete lattice. The macroscopic quantities that describe the fluid flow can be calculated as integrals of this distribution. Since the motion of

particles is limited to fixed paths connecting lattice nodes, the resolution process needs only information about nearest neighbor nodes. This feature, along with the explicit nature of the numerical scheme, makes LBMs very suitable for parallelization.

The lattice Boltzmann models seem to be very promising for the analysis of reactive mixtures in porous layers [37, 38]. For this reason, a lot of work has been performed in recent years in order to produce reliable lattice Boltzmann models for multi-component fluids and, in particular, for mixtures composed of miscible species [39–43]. The problem is to find a proper way, within the framework of a simplified kinetic model, for describing the interactions among different particles. Once this milestone is achieved, the extension of the model to reactive flows is straightforward [44, 45] and essentially involves additional source terms in the species equations which result from the reaction rate. Unfortunately most existing lattice Boltzmann models for mixtures are based on heuristic assumptions or prescribe too many constraints for setting the microscopic parameters, the end result of which is an idealized macroscopic description.

The ultimate goal of the present work is that of obtaining a complete mesoscopic model of fluid flow and reaction in three dimensional fuel cell porous media. The advantage of this would be that only the medium microstructure would need to be measured (for example by means of microscopic images and/or tomography scan) and then cell performance could be predicted. In the present paper the following concrete steps towards the achievement of this goal are discussed.

- Firstly, the reliability of the numerical simulations strongly depends on the reliability of the considered microscopic topology used in the simulations, i.e. if the microscopic topology actually reproduces the physical distribution of the solid phases. In this paper a three-dimensional microscopic topology was reconstructed based on the granulometry law. The intrinsic limits of this technique will be outlined.
- Secondly, the reactive mixture model [46] previously considered [47] was substituted with an updated model recently proposed [48, 49] which is based on the Gross & Krook model, in order to deal with reactive gas mixtures characterized by large mass ratios and non-fixed Schmidt number, like those involved in the fuel cell modeling.
- Thirdly, a new semi-implicit algorithm, called SILBE scheme [49], was implemented in the three-dimensional code for reducing the computational time, thus, enabling larger computational domain. In particular, some numerical results are reported for the 256^3 case (16.8 millions of cells).

RECONSTRUCTION OF MICROSCOPIC TOPOLOGIES

First of all, the microscopic topology of the material for the numerical simulation have to be obtained. For a wide range of materials, this can be achieved by computer tomography using X-ray absorption contrast (XCT). Unfortunately, materials with fine structures do not yield the necessary image quality when using XCT. In particular, non-destructive X-ray computed micro-tomography directly produces 3D pore space at resolutions of around a micron. For SOFC application, this resolution is not sufficient and reconstructions from reliable 2D techniques, such as standard and back scanning electron microscopy (SEM/BSEM), is the only viable alternative. New three-dimensional imaging techniques like phase contrast tomography [50] relying on the use of synchrotron radiation overcome this problem. However, conventional microscopic images of cross-sections are still cheaper, faster, and with less effort to get [51].

After the image acquisition, a model from stochastic geometry is adapted to the microstructure by fitting the model parameters. To this end, geometric characteristics of the microstructure are determined and the parameters of the model are chosen such that characteristic properties of the material (e.g. porosity or fiber radius distribution) are represented correctly.

There are two main techniques for dealing with this statistical regression:

- the granulometry law, which is based on the simplifying assumption that the porous medium is made of regular grain with a fixed known shape;
- the multiple–point statistics, which takes into account the neighboring information for producing more reliable reconstruction [52].

Essentially the multiple-point statistics is used, based on two-dimensional (2D) thin sections as training images, to generate 3D pore space representations. Assuming that the medium is isotropic, a 3D image can be generated that preserves typical patterns of the void space seen in the thin sections. The use of multiple-point statistics predicts long-range connectivity of the structures better than granulometry law. Essentially the algorithm is based on three steps: borrowing multiple-point statistics from 2D training images; pattern reproduction and final image processing, for improving local quality and consistency of the reconstruction. Since the implementation of the multiple-point statistics is currently under development, in this paper the simpler granulometry law was considered.

Let us consider the anode-side of a conventional electrolyte supported planar SOFC. The experimental data and the microscopic pictures obtained by means of the back scanning electron microscopy are taken from [53]. Information regarding the three dimensional porous structure of Ni-metal / YSZ-electrolyte cermet is obtained using the microscopic image of the porous anode obtained by a back scanning electronic microscope. The reference microscopic image used for computing the granulometry laws for both Ni and YSZ is shown in Fig 1. First of all, some threshold must be considered in order to automatically distinguish among the two solid phases and the free pores for the mixture fluid flow. This conversions from the original analogical image (characterized by all the possible values of the gray scale) to the final digital map, which allows one to recognize the nature of the involved materials, is effected by errors dealing with how to estimate the proper thresholds for each material. This is one the main source of errors in producing reliable post-processing of microscopic images.

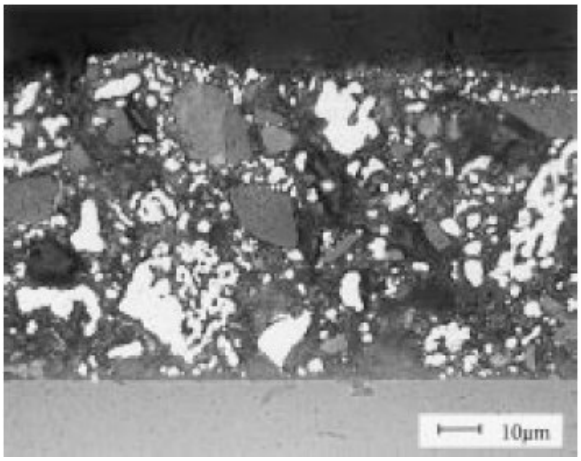

Figure 1. Micrograph of the Porous Anode (Bright: Ni, Grey: electrolyte, black: Pores) [53].

Once the digital map has been created, it is possible to compute the granulometry law. Essentially one must count how many grains, characterized by a given shape (square) and a given size, exist in the digital map. The procedure used to obtain the total number of grains of a particular grain size of a particular species is as follows:

- the whole computational domain is checked for the largest grain size possible;
- where ever the grain size is obtained the corresponding cells are converted to neutral cells (no more considered in the following computations);
- the number of grains corresponding to that particular grain size is counted;
- this procedure is repeated until the total count for least grain size of that species is obtained, in order to completely fill the whole surface occupied by a given species.

The results of the previous procedure are reported in the Fig. 2 for the Ni and in Fig. 3 for the YSZ. The granulometry laws for both materials are reasonably interpolated by exponential functions, namely

$$\left(\frac{N}{N_t}\right)_{Ni} = 0.4187 \cdot \exp\left(-0.6433 \cdot \frac{d}{d_0}\right) \quad (1)$$

$$\left(\frac{N}{N_t}\right)_{YSZ} = 0.2762 \cdot \exp\left(-0.6109 \cdot \frac{d}{d_0}\right) \quad (2)$$

where d_0 = 1 μm.

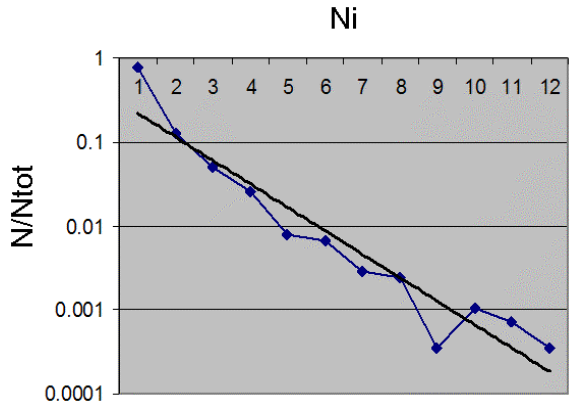

Figure 2. Granulometry law for Ni: relative populations with regards to the characteristic grain sizes for Ni.

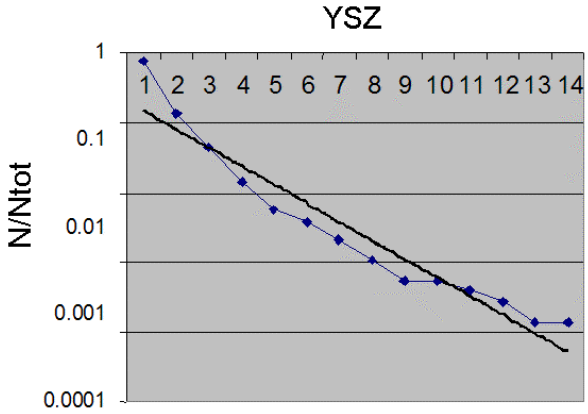

Figure 3. Granulometry law for YSZ: relative populations with regards to the characteristic grain sizes for YSZ.

Once the granulometry law is obtained for both the electron conducting grain distribution and the ion conducting grain distribution, this information is used to generate the random porous structure of the portion of the anode layer, where the three phase boundaries are located. A code was developed to create the porous structure. The procedure used to generate the porous structure is as follows:

- the computational domain is first filled with the largest possible electron conducting grains (calculated number of grains from the granulometry law);
- the next step is to randomly fill the remaining computational domain with the next largest electron conducting grains;
- this procedure is continued till the smallest electron conducting grains are filled up in the computational domain;
- the above three steps are carried out for the ion conducting grains to fill up the computational domain.

Some simple geometrical relations must be applied in order to ensure that the 3D reconstructed microscopic topology has the porosity experimentally measured. The final result of the 3D reconstruction procedure is reported in Fig. 4.

The next step is to locate the tree phase boundaries (TPBs), where the electrochemical reactions take place. For locating the TBPs, it is not enough to simply check where an electron conducting cell (ECC), an ion conducting cell (ICC) and a fluid path cell (FPC) are in contact with each other. In fact in order to realize an electrochemical reaction, the ECC must be in contact with the electron sink, i.e. the metal grid collecting the electrons on the anode-side of the fuel cells. This means that at least one connection path must exists between the collecting grid and the considered ECC. In a similar way, one must ensure that the ICC is physically connected with the electrolyte bulk and the FPC is connected with the gas supply/discharge network (otherwise the reactants and the products of the electrochemical reaction would not be available). This consistency condition is ensured by the reconstruction software by checking that three paths exist for ions, electrons and gasses respectively. If this condition is satisfied, then the corresponding location is marked as an active three phase boundary.

In the next section, the details of the physical model used for describing the fluid flow of the reactive mixture are discussed.

MATHEMATICAL MODEL FOR REACTIVE MIXTURE FLOW IN POROUS MEDIA

Continuous kinetic model

Following the derivation of the Boltzmann equation for a simple system with a single species, the kinetic equations for a simple system comprised of a mixture can be derived in a very similar way [54–56]. Let us consider a mixture composed of only two types of particles labeled *a* and *b*. The two Boltzmann equations for the binary system are

$$\frac{\partial f_A}{\partial t} + \mathbf{v} \cdot \nabla f_A + \mathbf{g}_A \cdot \nabla_{\mathbf{v}} f_A = Q_{AA} + Q_{AB}\,, \quad (3)$$

$$\frac{\partial f_B}{\partial t} + \mathbf{v} \cdot \nabla f_B + \mathbf{g}_B \cdot \nabla_{\mathbf{v}} f_B = Q_{BA} + Q_{BB}\,, \quad (4)$$

where $f_A(\mathbf{x}, \mathbf{v}, t)$ is the continuous single particle distribution function for the *a* species, $\mathbf{v}$ is the microscopic velocity, $\mathbf{g}_A$ is the acceleration due to an external field for the *A* species, and similar definitions hold for the *B* species too. The quadratic expressions

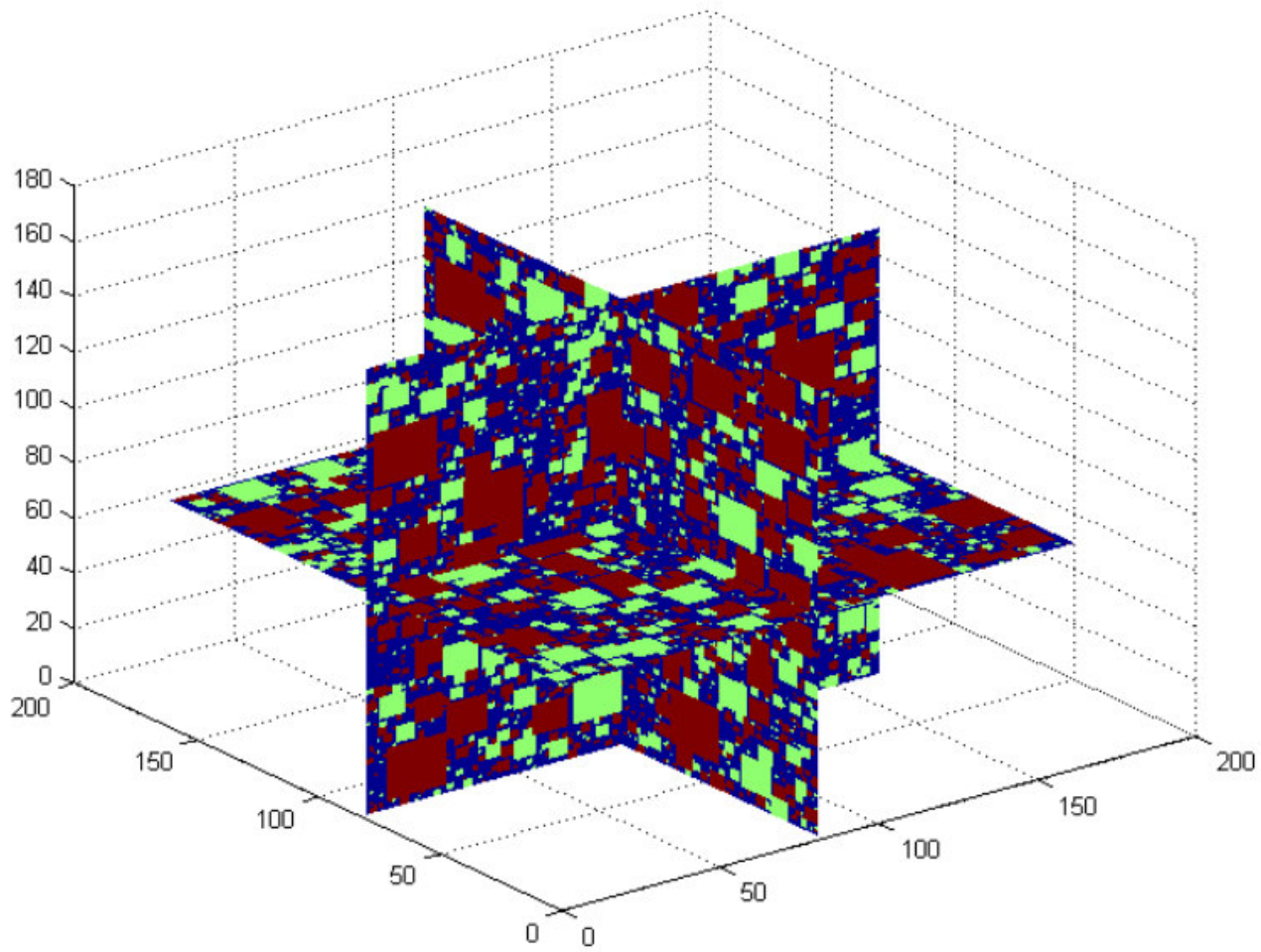

Figure 4. Reconstructed 3D microscopic topology used in the numerical simulations. The distribution of the three phases is consistent with the granulometry laws reported in Figs. 2 and 3, derived by the post-processing of the micrograph reported in Fig. 1.

Q_{AA} and Q_{BB} are the collisional terms which describe the c collisions among particles of the same type (*self-collisions*), while Q_{AB} and Q_{BA} are the collisional terms due to the interactions among different species (*cross-collisions*).

Each collision term has a well–known structure similar to the collision operator involved in the Boltzmann equation for a single fluid [31]. The time evolution of the distribution function for each species is affected both by collisions with particles of the same type and with particles of different type. These two phenomena are the kinetic driving forces of the equilibration process for the whole mixture.

A simplified kinetic model which allows one to separately describe both the driving forces, as they appear in the original Boltzmann equations, would be desirable. Essentially the key idea is to substitute the previous collisional terms with simplified ones, which are selected with a BGK–like structure. In particular, the BGK operator involves the difference between the actual value of the distribution function and the equilibrium one. Unfortunately there is considerably more latitude in the choice of a linearization procedure in the case of a mixture than for a pure gas [56]. In the latter case, a local Maxwellian centered on the (uniquely defined) macroscopic velocity is usually the candidate for the unperturbed component of the distribution function. In a mixture, however, it is possible to linearize about a local Maxwellian which contains the barycentric velocity or, alternatively, we can introduce distinct species flow velocities and linearize about local Maxwellians which contain these quantities.

Even though it could yield to slightly more complicated models, the choice of separate Maxwellians seems more general and better suitable for dealing with different regimes consistently. The model obtained is due to Hamel [57–59]. A Lattice Boltzmann formulation of this model has been recently proposed [46] and it was previously used for describing reactive mixtures [47].

Unfortunately the Hamel model (and all those coming from a proper linearization of it) are not completely consistent [48]. In fact if one sums over the species equations does not exactly recover the momentum equations (as it should be). Since the errors are negligible for fluid flows characterized by low Reynolds numbers, this model was considered in our preliminary simulations, because it allows one to tune the Schmidt number of the binary mixture (ratio between molecular diffusivity and mixture kinematic viscosity). Unfortunately the tuning strategy, i.e. finding the proper combination of relaxation parameters for achieving this goal, and the correction terms for compensating the discretization errors required some complicated algebra, which (unacceptably) increases the computational demand.

A new Lattice Boltzmann model was developed [49] for recovering the transport coefficients of real mixtures in a simpler way. The continuous (pseudo-) kinetic model used as the theoretical starting point is the model due to Gross & Krook [60]. Let us use $\sigma = A, B$ for indicating the generic species. The simplified kinetic equation has the general form

$$\frac{\partial f_\sigma}{\partial t} + \mathbf{v}\cdot\nabla f_\sigma + \mathbf{g}_\sigma \cdot \nabla_{\mathbf{v}} f_\sigma = -\frac{1}{\tau_m}\left[f_\sigma - f^e_{\sigma(m)} \right], \tag{5}$$

where τ_m is the relaxation time constant for cross-collisions and $f^e_{\sigma(m)}$ is a Maxwellian distribution function centered on a characteristic velocity for the mixture. The explicit expressions of this Maxwellian is

$$f^e_{\sigma(m)} = \frac{\rho_\sigma / m_\sigma}{(2\pi e_\sigma)^{D/2}} exp\left[-\frac{1}{2}\frac{(\mathbf{v}-\mathbf{u})^2}{e_\sigma} \right], \tag{6}$$

where ρ_σ is the generic species density, m_σ the particle mass, $\mathbf{u}$ is the macroscopic barycentric velocity, e_σ is the internal energy, and D the number of physical dimensions. The barycentric velocity is defined as

$$\mathbf{u} = \sum_\sigma x_\sigma \mathbf{u}_\sigma = \sum_\sigma \rho_\sigma \mathbf{u}_\sigma / \sum_\sigma \rho_\sigma \,, \tag{7}$$

where x_σ is the mass concentration (mass fraction) for the generic species. Local momentum conservation implies that the relaxation time constant τ_m for the cross-collisions must be the same for all species.

Macroscopic quantities, such as the density $\rho_\sigma(\mathbf{x},t)$, the macroscopic specific velocity $\mathbf{u}_\sigma(\mathbf{x},t)$, and, consequently, the macroscopic barycentric velocity $\mathbf{u}(\mathbf{x},t)$ can be calculated as the moments of the density distribution function, i.e.

$$\rho_\sigma(\mathbf{x},t) = \int_{-\infty}^{+\infty} m_\sigma f_\sigma \, d\mathbf{v} \,, \tag{8}$$

$$\rho_\sigma \mathbf{u}_\sigma(\mathbf{x},t) = \int_{-\infty}^{+\infty} m_\sigma \mathbf{v} f_\sigma \, d\mathbf{v} \,. \tag{9}$$

This model is truly much simpler than Hamel model, but it has only one tunable parameter, which is not enough for recovering both the desired molecular mixture diffusivity and the mixture kinematic viscosity. However this problem can be fixed once a proper discretization of the microscopic velocities (lattice) is considered.

Lattice kinetic model

To solve the continuous kinetic equation (equation (5)), the discrete ordinate method can be applied [60, 61]. According to this method, a set of discrete microscopic velocities $\mathbf{v}_i$ must be defined on which the distribution function is evaluated. The generic function $f^i_\sigma(\mathbf{x},t)$ is the single particle distribution function evaluated for velocity $\mathbf{v}_i$ at $(\mathbf{x},t)$. In the present paper, a three dimensional lattice called D3Q19, which makes use of nineteen discrete velocities, is considered [62]. The specific lattice used in the calculation is identified by the magnitude c (all the lattices in the same set have the same proportions among the elements but they are all scaled the physical microscopic velocity c, called lattice speed).

This assumption simplifies the development of the numerical code, and it is essential for the physical model, because the discrete lattice will be used for overcoming the intrinsic constraints of the continuous Gross & Krook model.

Thus, the kinetic equation, which is an integro-differential equation, reduces to a system of differential equations. The term that takes into account the effect of the external force field can be neglected, because we are interested in concentration driven flows (actually a proper forcing term is considered in the numerical implementation for improving the accuracy of the method). Since the reference lattice has been defined, it is possible to write the operative formula in vectorial form, namely

$$\frac{\partial \mathbf{f}_\sigma}{\partial t} + \mathbf{V}\cdot\nabla\mathbf{f}_\sigma = \mathbf{A}_m\left[\mathbf{f}^e_{\sigma(m)} - \mathbf{f}_\sigma \right], \tag{10}$$

where $\mathbf{V}$ is the matrix collecting all the lattice components ($\mathbf{V} \in \mathbb{R}^{Q\times D} = \mathbb{R}^{19\times 3}$) and the scalar product between matrices must be thought as saturating the second index (in fact $\nabla\mathbf{f}_\sigma \in \mathbb{R}^{19\times 3}$ and consequently $\mathbf{V}\cdot\nabla\mathbf{f}_\sigma \in \mathbb{R}^{19\times 1}$).

According to the Gross & Krook model on a lattice, the collisional matrix should be diagonal, namely $\mathbf{A}_m = \lambda_m \mathbf{I}$, where $\lambda_m = 1/\tau_m$. However for increasing the number of tunable parameter, the collisional matrix is assumed as

$$\mathbf{A}_m = \mathbf{M}_D^{-1}\mathbf{D}_m\mathbf{M}_D \,, \tag{11}$$

where $\mathbf{M}_D$ defines a proper ortho-normal basis[1] for the D3Q19 lattice and $\mathbf{D}_m$ is the diagonal matrix, namely

$$\begin{aligned} diag(\mathbf{D}_m) = [&0, \lambda_m^I, \lambda_m^I, \lambda_m^I, \lambda_{m1}^{II}, \lambda_{m1}^{II}, \lambda_{m1}^{II}, \lambda_{m1}^{II}, \lambda_{m1}^{II}, \lambda_{m2}^{II}, \\ &\lambda_m^{III}, \lambda_m^{III}, \lambda_m^{III}, \lambda_m^{III}, \lambda_m^{III}, \lambda_m^{III}, \lambda_m^{IV}, \lambda_m^{IV}, \lambda_m^{IV}] \end{aligned}, \tag{12}$$

collecting the generalized relaxation frequencies for self and cross collisions. As it will be clear later on (see the section concerning the numerical implementation), λ_m^I controls the molecular diffusivity, λ_{m1}^{II} and λ_{m2}^{II} control the mixture kinematic and bulk viscosity respectively, while λ_m^{III} and λ_m^{IV} are free parameters effecting the stability of the model (usually $\lambda_m^{III} = \lambda_m^{IV} = 1$).

Since only the distribution functions for discrete microscopic velocities are considered, an interpolation test function must be adopted to calculate the macroscopic quantities. In this way, the previous integrals (equations (8) and (9)) reduce to weighted summations of the considered discrete functions. The interpolation test function should be as similar to the Maxwellian distribution function as possible in order to easily include the equilibrium conditions. If we consider a low Reynolds number flow ($|\mathbf{u}_\sigma| \ll |\mathbf{v}|$), which essentially means $U \ll c$, the equilibrium distribution function can be linearized around the state at rest [41]. This assumption allows one to compute the lattice weights for performing the calculation of the macroscopic quantities. The final result is that all the macroscopic (both hydrodynamic and not-conserved) moments are proper linear combinations of the discrete distribution functions, or, equivalently, a linear mapping exists

[1] Details on how to derive the ortho-normal basis are reported in [A3]. Even though this paper discusses the two dimensional case (D2Q9 lattice), the derivation technique for the three dimensional case is the same. The transformation matrix is made of (simple) numerical constants.

between the macroscopic moments and the discrete distribution functions.

Once the hydrodynamic moments are computed, we need to verify that they satisfy the desired macroscopic transport equations. For achieving this goal, the diffusive scaling [64] can be properly applied. There are three characteristic time scales in this system: the time scale T_C, which properly describes the collision phenomenon, i.e. $O(\tau_m / T_C) = 1$; the time scale T_F, which properly describes the particle dynamics on the lattice, i.e. $O[(L/c)/T_F] = 1$ where L is the system size and, finally, the time scale T_S, which properly describes the slow fluid dynamics, i.e. $O[(L/U)/T_S] = 1$. The fast fluid dynamics (acoustic waves) was neglected. Since a lot of collisions are needed in order to travel across the system, then $T_C / T_F = \varepsilon$, where ε. Moreover since $U/c \ll 1$, then $T_F / T_S = \varepsilon$ and consequently $T_C / T_S = \varepsilon^2$. Once the characteristic time scales are defined, the basic idea is to express the previous equation in terms of some normalized quantities, in order to analyze the slow fluid dynamics only.

Applying the diffusive scaling to equation (10) for a binary mixture yields

$$\frac{\partial \rho_A}{\partial t} + \nabla \cdot (\rho_A \mathbf{u}_A) = 0 , \tag{13}$$

$$\frac{\partial \rho_B}{\partial t} + \nabla \cdot (\rho_B \mathbf{u}_B) = 0 , \tag{14}$$

$$\rho_A (\mathbf{u}_A - \mathbf{u}) = -D_A \nabla \rho_A , \tag{15}$$

$$\rho_B (\mathbf{u}_B - \mathbf{u}) = -D_B \nabla \rho_B , \tag{16}$$

$$\frac{\partial \rho \mathbf{u}}{\partial t} + \nabla \cdot (\rho \mathbf{u} \otimes \mathbf{u}) = \nabla p + \nu \rho \left(\nabla \mathbf{u} + \nabla \mathbf{u}^T \right) , \tag{17}$$

where $D_A = e_A / \lambda_m^I$, $D_B = e_B / \lambda_m^I$, $\nu = c^2 / (3 \lambda_{m1}^{II})$ and

$$\begin{aligned} p &= p_A + p_B \\ p_A &= e_A \rho_A \\ p_B &= e_B \rho_B \end{aligned} . \tag{18}$$

The internal energies (since this is an athermal model, the concept of internal energy is not rigorously defined) can be expressed by means of the molecular weights, namely $e_A = RT / M_A$ and $e_B = RT / M_B$, where T is the temperature and R is the universal gas constant (8.31441 J mol^{-1} K^{-1}). Consequently it is possible to define an equivalent molecular weight for the mixture in such a way that $p / \rho = RT / M$, where

$$M = \frac{1}{x_A / M_A + x_B / M_B} . \tag{19}$$

This equivalent molecular weight for the mixture depends on the local concentrations ($x_A = \rho_A / \rho$ and $x_B = \rho_B / \rho$), because it is not an intrinsic property of the components. By applying the previous definitions, the species diffusion velocities can be rewritten as

$$\rho_A (\mathbf{u}_A - \mathbf{u}) = -\rho D \nabla x_A - D \frac{x_A x_B (M_B - M_A)}{x_A M_A + x_B M_B} \nabla \rho , \tag{20}$$

$$\rho_B (\mathbf{u}_B - \mathbf{u}) = -\rho D \nabla x_B + D \frac{x_A x_B (M_B - M_A)}{x_A M_A + x_B M_B} \nabla \rho . \tag{21}$$

Before proceeding in this direction, it is worth highlighting that the macroscopic equations which derive from the lattice kinetic model do not involve chemical reactions, because there is no source term in the continuity equation. The electrochemical reactions realize a concentration driven flow by modifying the species concentrations at the three phase boundaries, while there are no chemical reactions in the fluid bulk. For this reason, the electrochemical reactions were simply modeled by means of proper boundary conditions with regards to the concentration for the fluid cells close to the three phase boundaries.

Numerical algorithm

First of all, in order to develop the operative formulas for the numerical implementation, the lattice equilibrium distribution functions can be explicitly expressed as

$$\left[\mathbf{f}^e_{\sigma(m)} \right]_i = \rho_\sigma s_I^i \left[\frac{s_0^i}{s_I^i} + \frac{3}{c^2} \mathbf{v}_i \cdot \mathbf{u} + \frac{9}{2c^4} (\mathbf{v}_i \cdot \mathbf{u})^2 - \frac{3}{2c^2} \mathbf{u}^2 \right] , \tag{22}$$

where $\mathbf{v}_i \in \mathbf{V}$ is the i-th lattice velocity, while the two sets of constants, namely

$$\begin{aligned} \mathbf{s}_0 = [& 1\text{-}2/3 s_\sigma, 1/18 s_\sigma, 1/18 s_\sigma, 1/18 s_\sigma, 1/18 s_\sigma, \\ & 1/36 s_\sigma, 1/36 s_\sigma, 1/36 s_\sigma, 1/36 s_\sigma, 1/36 s_\sigma, 1/36 s_\sigma, 1/36 s_\sigma, , \\ & 1/36 s_\sigma, 1/18 s_\sigma, 1/36 s_\sigma, 1/36 s_\sigma, 1/36 s_\sigma, 1/36 s_\sigma, 1/18 s_\sigma] \end{aligned} \tag{23}$$

and $\mathbf{s}_I = \mathbf{s}_0 (s_\sigma = 1)$, are functions of the ratio $s_\sigma = 3 e_\sigma / c^2$.

It is clear from equation (22) that it is possible to distinguish in the equilibrium distribution functions terms which do not depend ($\mathbf{f}^{e0}_{\sigma(m)}$) or depend linearly ($\mathbf{f}^{e1}_{\sigma(m)}$) on the mixture velocity. Both these terms can be expressed by means of a linear mapping of the actual distribution functions (the equilibrium distributions depend on the moments and the latter are linear combinations of the actual distribution functions), namely

$$\mathbf{f}^{e0}_{\sigma(m)} = \mathbf{M}_{e0} \mathbf{f}_\sigma , \tag{24}$$

$$\mathbf{f}^{e1}_{\sigma(m)} = x_\sigma \mathbf{M}_{e1} \sum_\sigma \mathbf{f}_\sigma . \tag{25}$$

Consequently the residual quadratic terms can be expressed as

$$\mathbf{f}^{e2}_{\sigma(m)} = \mathbf{f}^{e}_{\sigma(m)} - \mathbf{f}^{e0}_{\sigma(m)} - \mathbf{f}^{e1}_{\sigma(m)} . \tag{26}$$

Secondly some dimensionless coordinates can be considered (the so-called "lattice units"). Let us introduce a dimensionless space $\hat{x} = x / L$, time $\hat{t} = t / T_S$ and collisional operator, namely $\hat{\mathbf{A}}_m = T_C \mathbf{A}_m$. In this dimensionless system, the continuous formula given by equation (10) can approximated by the following discrete formula on a regular spatial mesh, namely

$$\mathbf{f}_\sigma (\hat{t}, \hat{\mathbf{X}}) - \mathbf{f}_\sigma (\hat{t} - 1, \hat{\mathbf{X}} - \hat{\mathbf{V}}) = \hat{\mathbf{A}}_m \left[\mathbf{f}^e_{\sigma(m)} (\hat{t}, \hat{\mathbf{X}}) - \mathbf{f}_\sigma (\hat{t}, \hat{\mathbf{X}}) + \mathbf{k}_b (\hat{t}, \hat{\mathbf{X}}) \right] \tag{27}$$

where $\mathbf{k}_b (\hat{t}, \hat{\mathbf{X}})$ is a proper forcing term, which must be introduced in order to satisfy the continuity equations with the discrete formula up to the second order in space and first order in time (see [A3] for details). The previous integration rule derives

directly from the implicit backward Euler formula. The implicit formulation allows one to improve the stability of the scheme, i.e. for any values of the relaxation frequencies the macroscopic transport coefficients can not assume unphysical (negative) values.

Unfortunately the implicit formulation is computationally more demanding and, for this reason, the improved stability must be paid by a longer simulations. However in this case it is possible to develop a semi-implicit formulation, i.e. it is possible to compute implicitly all the terms which can be solved once for all the beginning of the computations (pre-processing) and explicitly only the quadratic terms. The reason is that the quadratic terms do not effect much the stability performance.

The first step is to derive a operative formula for the barycentric distribution function, which is computed by the sum of the species distribution functions. Substituting equations (24, 25, 26) into equation (27) and summing over all the species yields

$$\sum_{\sigma} \mathbf{f}_{\sigma}(\hat{t},\hat{\mathbf{X}}) = \mathbf{B}_S \sum_{\sigma} \mathbf{f}_{\sigma}(\hat{t}-1,\hat{\mathbf{X}}-\hat{\mathbf{V}}) + \mathbf{B}_Q \sum_{\sigma} \mathbf{f}^{e2}_{\sigma(m)}(\hat{t}-1,\hat{\mathbf{X}}) \,, \quad (28)$$

where

$$\mathbf{B}_S = \left[\mathbf{I} - \hat{\mathbf{A}}_m\left(\mathbf{M}_{e0} - \mathbf{I}\right) - \hat{\mathbf{A}}_m \mathbf{M}_{e1}\right]^{-1}, \quad (29)$$

and $\mathbf{B}_Q = \mathbf{B}_S \hat{\mathbf{A}}_m$.

Once that the barycentric distribution function is known, i.e. $\sum_{\sigma} \mathbf{f}_{\sigma}(\hat{t},\hat{\mathbf{X}})$, then it is possible to solve the equation for each species distribution function (actually it is enough to solve N-1 equations if N is the number of species because the residual can be deduced by the barycentric conditions), namely

$$\begin{aligned} \mathbf{f}_{\sigma}(\hat{t},\hat{\mathbf{X}}) = \mathbf{S}_S \mathbf{f}_{\sigma}(\hat{t}-1,\hat{\mathbf{X}}-\hat{\mathbf{V}}) + \mathbf{S}_Q \mathbf{f}^{e2}_{\sigma(m)}(\hat{t}-1,\hat{\mathbf{X}}) \\ + x_{\sigma}(\hat{t},\hat{\mathbf{X}}) \mathbf{S}_C \sum_{\sigma} \mathbf{f}_{\sigma}(\hat{t},\hat{\mathbf{X}}) \end{aligned} \,, \quad (30)$$

where

$$\mathbf{S}_S = \left[\mathbf{I} - \hat{\mathbf{A}}_m\left(\mathbf{M}_{e0} - \mathbf{I}\right) + \frac{\lambda^I_m}{2-\lambda^I_m} \hat{\mathbf{A}}_m \mathbf{M}_{e1}\right]^{-1}, \quad (31)$$

$\mathbf{S}_Q = \mathbf{S}_S \hat{\mathbf{A}}_m$ and $\mathbf{S}_C = 2/(2-\lambda^I_m)\mathbf{S}_S \hat{\mathbf{A}}_m \mathbf{M}_{e1}$. This equation is very similar to the previous equation (28), with the exception of an additional coupling term for taking into account the effects due to the transport of mixture barycentric properties (computed in the previous step). The last term in the matrix given by equation (31) must compensate the additional forcing term $\mathbf{k}_b(\hat{t},\hat{\mathbf{X}})$ introduced in the operative formula for satisfying the continuity equation with more accuracy.

The quadratic terms are the only ones explicitly computed. The generic concentration $x_{\sigma}(\hat{t},\hat{\mathbf{X}})$ can be immediately computed at the new time step by means of $\mathbf{f}_{\sigma}(\hat{t}-1,\hat{\mathbf{X}}-\hat{\mathbf{V}})$ because the collisional operator conserves the density (because of the diffusion phenomenon, the density is the only conserved moment in this case).

The outlined numerical algorithm reproduces the actual dynamics of mass transport phenomena: the barycentric velocity field is solved first because it is the leading term and then the diffusion velocities for each species follow. All the previous matrices $\mathbf{B}_S$, $\mathbf{B}_Q$, $\mathbf{S}_S$, $\mathbf{S}_Q$ and $\mathbf{S}_C$ depend only on the dimensionless relaxation frequencies: hence they can be computed one for all at the beginning of the calculation, being the same for all the computational cells.

Practical issues of implementation

First of all, some coding tricks must be considered in order to increase the performance of the code executed on a single machine.

The matrix notation is useful for explaining the essential features of the method and to analytically deduce the numerical accuracy of the scheme. However the direct implementation of the matrix formulation in the numerical code is highly inefficient. For this reason, all the previously outlined operations are directly implemented in order to outline the common terms. In particular the common sub-expression elimination (CSE) was used in the design of the numerical code. Even though modern compilers include automatically this feature, an accurate design of the code allows one to take specific advantages from the Lattice Boltzmann formulation. For example, performing the collision step in moment space (defined by a proper linear mapping applied to the conventional space) reduces the number of required operations. Moreover eliminating the moment calculation as a separate step allows one to reduce the memory access time.

Dealing with large computational domain (256^3 = 16.8 millions of cells and more), the code parallelization is mandatory. In particular, the code has been developed in C++ and a free communication library has been adopted (MPICH 1.3) based on MPI technology [65]. The reported numerical results were obtained on a Virginia Tech (VT) cluster facility, which is essentially a 2200 node Mellanox switches / Cisco Gigabit Ethernet cluster, called SYSTEM X. The typical number of CPUs used in the simulations was 64. Since an elementary decomposition was used, more computational nodes would produce a reduction in the parallelization efficiency (see [47]), because the decomposed computational domain may have a local porosity which differs from the global one and this yields to load unbalance.

The speed performance of the code were measured during the present tests by the actual MLUPS. Let us introduce the million of lattice updates per second $\dot{N}_{UP}$ (measured in MLUPS) as an useful parameter for estimating the code performance independently from the number of used nodes, namely

$$\dot{N}_{UP} = \frac{\varepsilon D^3 N_F N_C}{N_{CPU} Time} \,, \quad (32)$$

where ε is the porosity, D is the edge dimension of the cubic computational domain, N_F is the number of fluids, N_C is the number of collisions and N_{CPU} is the number of CPUs. Typical values for this parameter are close to 0.3 MLUPS, which is slightly slower than other numerical codes developed for solving reactive mixtures in porous media. The reason is due to the fact the semi-implicit formulation is 25 % slower than conventional explicit formulation. For the present application, the stability of the method was privileged.

First of all, the computational domain given by Fig. 4 is refined, which means that the computational mesh is denser than the physical grid used for defining the porous medium, in order to ensure that the numerical results are mesh independent. Usually the fluid flow in each physical cell used to describe the porous medium is solved by means of 8^3 = 512 computational cells. The typical domain decomposition for 64 CPUs is reported in Fig. 6 together with a brief schematic of the species flow directions.

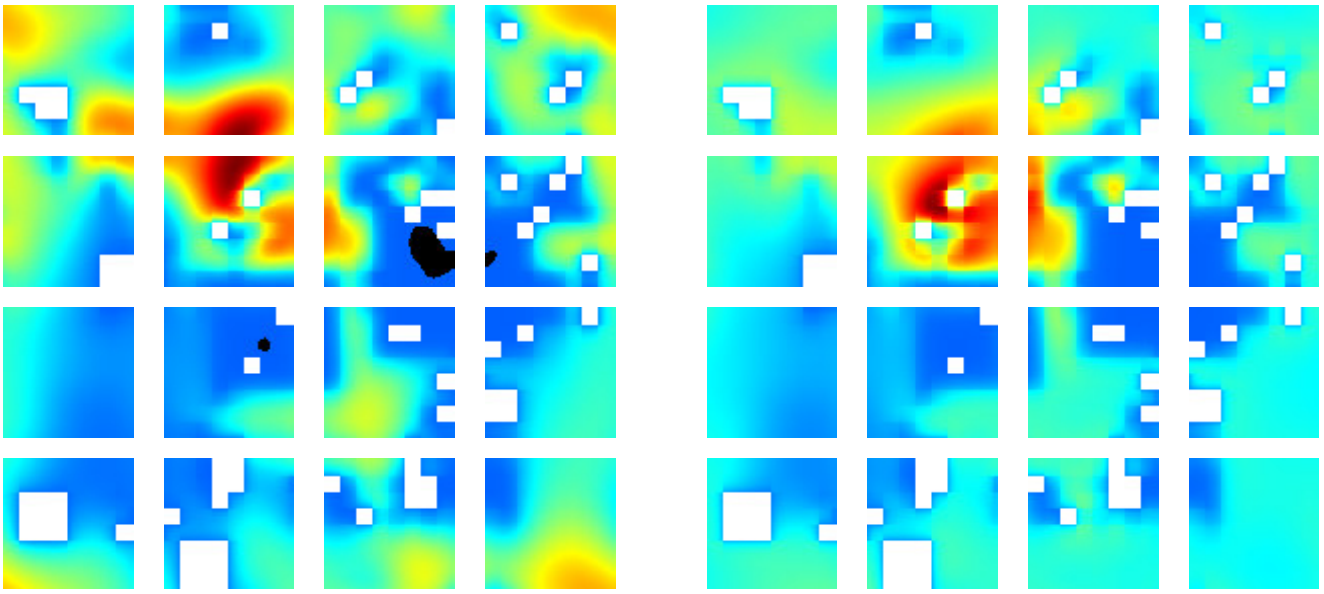

Figure 5. Contours of the mass fluxes at the main I/O bottom plane (moving orthogonal to the picture): on the left hand side, out-coming (with regards to the porous anode) mass fluxes for the water produced by the electrochemical reactions (the black regions are where the flux is reversed due to drag effect), while, on the right hand side, in-coming mass fluxes for the consumed hydrogen.

NUMERICAL RESULTS AND CONCLUSIONS

In the usual macroscopic modeling, some mass transport models inside the porous SOFC anode must be applied to estimate gas concentrations at the anode–electrolyte interface. However, such a mass transport model needs to be sophisticated enough so that it can take into account parameters such as complex functions of temperature, pressure, gas concentrations, and the physical properties of SOFC materials like porosity, tortuosity and pore size of the electrode materials [66]. The essential problem is that all these models depend somehow on fitting parameters.

In general, mass transport of components inside porous media can be described using either the extended Fick model (EFM) or the dusty gas model (DGM). Both FM and the DGM are mass transport equations taking into account Knudsen diffusion, molecular diffusion and the effect of a finite pressure gradient. Some other authors eliminated out the effect of Knudsen diffusion leaving on by the Stefan–Maxwell model in their mass transport equations (SMM).

There are some evident degrees of freedom in selecting the fitting parameters concerning the porous medium microstructure in order to recover the experimental data. Moreover the application of the previous models deal some additional simplifications. For example, it is quite popular to neglect the effects due to the finite pressure gradient. This hypothesis seems reasonable since there is no net change in the number of moles in the gas phase due to electrochemical reactions. From the practical point of view, this means neglecting the second terms at the right hand side in equations (19, 20). Unfortunately this assumption is not acceptable. The fact that the total number of moles in the gas phase does not change does not necessarily implies that the pressure is constant. In fact the total mixture mass increases due to the electrochemical reactions (we are substituting lighter hydrogen particles with heavier water particles) and, for this reason, a net out-coming mass flux must exist in steady state conditions. This is understandable if we take into account that a relevant mass flux is entering by means

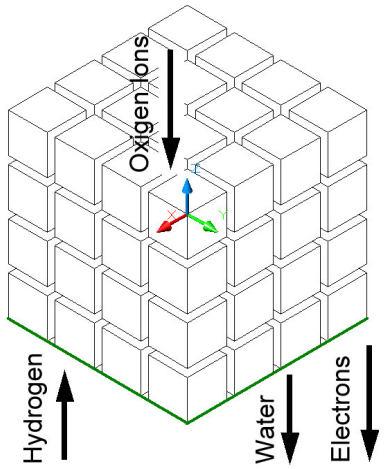

Figure 6. Brief schematic of the considered application decomposed on 64 computational processes. The species flow directions and the main I/O bottom plane are outlined.

Table 1. Molecular properties for binary mixtures of H_2 / H_2O.

T	ν	D	Schmidt
[°C]	[m^2/s]	[m^2/s]	[-]
500	0.000118	0.000201	1.699
600	0.000164	0.000279	1.699
700	0.000216	0.000367	1.699
800	0.000273	0.000463	1.700
900	0.000334	0.000568	1.701
1000	0.000400	0.000681	1.702
1100	0.000471	0.000802	1.704

of the (heavy) ions moving in the electrolyte. In other words, there is a relevant out-coming mixture flux and consequently a proper total pressure gradient must exist for ensuring the driving force of this flow.

The goal of the reported calculations is to directly solve the fluid flow of reactive mixtures in porous anodes. First of all, the transport coefficients must be tuned according to the (pure) molecular values coming form the kinetic theory. These input data must be the same considered by the macroscopic approaches in order to make the comparison more reliable.

First of all, we have to deal with a very large mass particle ratio (M_{H2O}/M_{H2} = 9) by essentially tuning the fraction of moving particles with regards to those at rest. Recalling that

$$e_A = \frac{RT}{M_A} = s_A \frac{c^2}{3}, \tag{33}$$

$$e_B = \frac{RT}{M_B} = s_B \frac{c^2}{3}, \tag{34}$$

it is possible to tune s_A = 1.00, and consequently c = 3685.8 m/s and s_B = 0. 11. The corrective factor for the mixture equations (barycentric flux) is slightly more complicated, namely

$$s = s_A \left(x_A + \frac{M_A}{M_B} x_B \right), \tag{35}$$

because it depends on the local concentrations (in this case s^0 = 0.20 only at the beginning of the calculations and at the I/O bottom plane).

Concerning the transport coefficients, the mutual ordinary diffusivity can be expressed by [67]

$$D = \frac{C}{p\sigma_{AB}^2 \Omega_D} \sqrt{T^3 \frac{M_A + M_B}{M_A M_B}}, \tag{36}$$

while the mixture kinematic viscosity can be expressed by

$$\nu = \frac{x_A \nu_A}{1 + F_{AB}(M_A/M_B)(x_B/x_A)} + \frac{x_B \nu_B}{1 + F_{BA}(M_A/M_B)(x_A/x_B)}. \tag{37}$$

Consequently the Schmidt number, defined as $Sc = \nu / D$, can be computed. The transport properties computed by means of equations (33, 34) are reported for in Table 1 for a mixture with 10 % in mass of hydrogen. This concentration is assumed as initial condition for the numerical simulations and the transport coefficients are kept fixed during the simulations (the actual concentrations are very close to this condition).

Taking into account the expressions derived by means of the asymptotic analysis, it is possible to correlate the dimensionless mutual diffusivity with the first dimensionless relaxation frequency, namely

$$\hat{D} = \frac{D}{c^2 T_C} = \frac{1}{3\hat{\lambda}_m^I} \frac{\left(x_A M_A + x_B M_B\right)}{M_B}, \tag{38}$$

or equivalently

$$\hat{\lambda}_m^I = \frac{\left(x_A M_A + x_B M_B\right)}{3 M_B \hat{D}}. \tag{39}$$

For the mixture kinematic viscosity, a similar procedure can be considered with the difference that an additional term due to the artificial numerical viscosity must be included (preserving the fact that this coefficient must be always positive), namely

$$\hat{\nu} = \frac{\nu}{c^2 T_C} = \frac{1}{3\hat{\lambda}_{m1}^{II}} \left(1 + \frac{\hat{\lambda}_{m1}^{II}}{2} \right), \tag{40}$$

or equivalently

$$\hat{\lambda}_{m1}^{II} = \frac{1}{3\hat{\nu} - 1/2}. \tag{41}$$

Finally, a proper set of boundary conditions must be considered. Since the computational domain is chosen to be smaller than the physical thickness of the anode layer, periodic geometric conditions are considered. This means that it must be imagined that the computational domain must be repeated in all directions in order to create the actual physical topology.

The electrochemical reactions do not act in the bulk fluid but only in the boundary fluid cells close to an (active) three phase boundary. The practical effects on the electrochemical reactions is to modify locally the species concentration and hence to produce concentration driven flow. It is easy to correlate the total inlet / outlet fluxes with the averaged operative conditions of the fuel cells by means of the current density J [68], namely

$$< \rho_A \mathbf{u}_A > = + M_A \frac{J}{2F}, \tag{42}$$

$$< \rho_B \mathbf{u}_B > = - M_B \frac{J}{2F}, \tag{43}$$

$$< \rho \mathbf{u} > = \left(M_A - M_B\right) \frac{J}{2F} < 0, \tag{44}$$

where $<\cdot>$ means spatially averaged quantity at the I/O bottom plane (see Fig. 6) and F is the Faraday constant (F = 96500 C mol^{-1}). From the previous expressions, it is easy to prove that, for a fixed current, the net out-coming mass flux is 8=(18-2)/2 times larger than the in-coming one. For this reason, a total pressure gradient must exist for ensuring the corresponding driving force.

The actual species concentrations close to the (active) three phase boundaries must be in such a way to generate the mass fluxes given by equations (42, 43, 44). Instead of using an iterative procedure (more computational demanding), the following strategy is suggested. Let us suppose that all the reactive cells behaves in the same way (homogeneous electrochemical reactions). The local species densities for the generic reactive cells, can be expressed as

$$\rho_A^R = \rho_A^0 - \delta\rho_D, \tag{45}$$

$$\rho_B^R = \rho_B^0 + \frac{M_B}{M_A}\left(\delta\rho_D + \delta\rho_M\right), \tag{46}$$

where $\delta\rho_D$ and $\delta\rho_M$ are free tunable parameters, while ρ_A^0 and ρ_B^0 are the fixed densities at the I/O bottom plane. The ratio M_B / M_A has been introduced in order to effect directly the partial pressures (in fact the densities must be divided by the

corresponding molecular weights for obtaining the partial pressure).

The numerical simulations confirm that the relation between the mass fluxes and the tunable parameters used for specifying the density in the reaction fluid cells is linear, namely

$$< \rho_A \mathbf{u}_A > - x_A^0 < \rho \mathbf{u} >= k_D \delta\rho_D \,, \tag{47}$$

$$< \rho_B \mathbf{u}_B > - x_B^0 < \rho \mathbf{u} >= -k_D \delta\rho_D \,, \tag{48}$$

$$< \rho \mathbf{u} >= -k_M \delta\rho_M \,, \tag{49}$$

where k_D and k_M are fitting parameters which can be measured by means of the numerical simulations. Recalling equations (42, 43) and substituting them into the previous equations yields

$$\begin{bmatrix} < \rho_A \mathbf{u}_A > \\ < \rho_B \mathbf{u}_B > \end{bmatrix} = \begin{bmatrix} k_D & -x_A^0 k_M \\ -k_D & -x_B^0 k_M \end{bmatrix} \begin{bmatrix} \delta\rho_D \\ \delta\rho_M \end{bmatrix} = \frac{J}{2F} \begin{bmatrix} M_A \\ -M_B \end{bmatrix}, \tag{50}$$

and consequently

$$\begin{bmatrix} \delta\rho_D \\ \delta\rho_M \end{bmatrix} = \frac{J}{2F} \begin{bmatrix} k_D & -x_A^0 k_M \\ -k_D & (x_A^0 - 1) k_M \end{bmatrix}^{-1} \begin{bmatrix} M_A \\ -M_B \end{bmatrix}, \tag{51}$$

which allows one to select the free tunable parameters on the local densities for the reactive cells in order to produce some mass fluxes coherent with a given current density. The simulations can be performed in three steps:

- first, some guessed values for the tunable free parameters $\delta\rho_D$ and $\delta\rho_M$ are assumed;
- then the fitting parameters k_D and k_M (for the specific porous medium) are computed;
- finally, the actual current density (homogeneously distributed) can be simulated by means of equation (50).

The last detail concerns how to recover the averaged mixture molecular weight. Recalling equation (34) and substituting equations (44, 45), yields

$$s(\mathbf{X}) = s^0 \frac{\rho^0}{\rho(\mathbf{X})} + \frac{\delta\rho_M M_A}{\delta\rho_M (M_B - M_A) + \delta\rho_M M_B} \left[1 - \frac{\rho^0}{\rho(\mathbf{X})} \right]. \tag{52}$$

In this way, the barycentric mass flux depends only on $\delta\rho_M$, because the tunable parameter $\delta\rho_D$ produces a concentration field characterized by a fixed total pressure and hence it should not produce any effect on the barycentric mass flux.

For proving the effectiveness of the discussed technique in simulating reactive mixtures for SOFCs, the following example is reported. The smallest grain used in the definition of the porous medium reported in Fig. 4 is 0.493 micron. A refinement factor of 8 was used in the numerical simulations, because it ensure mesh independent results. This implies that the smallest computational cell is 0.062^3 micron^3. The total size of the computational domain is 256^3 and it was solved on 64 CPUs. Hence each cube of the split domain reported in Fig. 6 is 64^3. The number of collisions required to produce steady state conditions was roughly 60,000 (15 hours of wall clock time on the cluster).

The reactive boundary conditions was tuned for modeling a current density equal to J = 0.4 A cm^{-2}, which is a typical value for this technology. In Fig. 5, the contours for the mass fluxes at the main I/O bottom plane (moving orthogonal to the picture) are reported: in particular on the left hand side, out-coming (with regards to the porous anode) mass fluxes for the water produced by the electrochemical reactions are showed (the black regions are where the flux is reversed due to drag effect), while, on the right hand side, in-coming mass fluxes for the consumed hydrogen are instead considered.

First of all, it is clear that at microscopic level the actual fluid flow is far from being homogeneous and it is much more complicate than what claimed by the averaged description used at macroscopic level. As far as the local optimization of the materials is not concerned, the macroscopic description does not need to get involved in so many details. However the optimization of the microscopic paths for both species would obviously produce an increase in the macroscopic performance. For example the numerical simulations show that the reconstructed portion of the porous medium has an high reactive core surrounded by less reactive portions. It is possible to imagine (at least in principle) to locate the solid phases in such a way to induce the suction flow of hydrogen in the central portion and the exhaust of water from the neighboring regions: in this way, the two species do not interfere with each other.

Even though the reported results are preliminary, they allow not to qualitatively investigate how the electrochemical reaction affects the hydrodynamics inside the porous anode layer at the microscopic level. In particular, this proves that the usual practice of separately investigating the hydrodynamics and electrochemistry seems somehow artificial and far from what actually happens microscopically.

Acknowledgments

V.K. would like to thank Prof. Michele Calì for offering him the opportunity for spending time at Politecnico di Torino, during which part of this work was done. V.K. would also like to thank Prof. Romano Borchiellini for his support at Politecnico. P.A. would like to thank Dr. Marco Coppo for his support during early coding phase.

Nomenclature

A	: geometrical area
c	: lattice speed
D	: mutual diffusivity
e	: specific internal energy
f	: continuous single particle distribution function
F	: Faraday's constant
g	: acceleration due to an external field
J	: electric current density
k	: kinetic forcing term
L	: length
m	: single particle mass
M	: molecular mass
Q	: collisional operator
R	: universal gas constant
T	: temperature
t	: time
u	: macroscopic velocity
v	: microscopic velocity
δ	: discrete step
ε	: porosity
λ	: relaxation frequency
ν	: kinetic viscosity
ρ	: density
τ	: collision time

Subscripts and superscripts

A	: generic species
B	: generic species
e	: equilibrium
m	: mixture
0	: value at I/O bottom value
σ	: generic species

REFERENCES

[1] Larminie, J., Dicks, A.L., "Fuel Cells Systems Explained", Wiley, New York, 2000.

[2] S. Srinivasan, R. Mosdale, P. Stevens, C. Yang, "Fuel cells: Reaching the era of clean and efficient power generation in the twenty-first century", Annual Review of Energy and the Environment, vol. 24, pp. 281-328, 1999.

[3] F.J. Gardner, "Thermodynamic processes in solid oxide and other fuel cells", Proceedings of the Institution of Mechanical Engineers, Part A: Journal of Power and Energy, vol. 211, n. 5, pp. 367-380, 1997.

[4] Singhal S.C., "Advances in solid oxide fuel cell technology", Solid State Ionics, vol. 135, pp. 305-313, 2000.

[5] McEvoy A.J., "Thin SOFC electrolytes and their interfaces – A near-term research strategy", Solid State Ionics, vol. 132, pp.159-165, 2000.

[6] T. Ackmann, L.G.J. Haart, W. Lehnert, F. Thom, "Modeling of mass and heat transport in thick-substrate thin-electrolyte layer SOFCs", proceedings of the 4th European Solid Oxide Fuel Cell Forum, Lucerne/Switzerland, pp. 431-438, 2000.

[7] Weber et Al., "Materials and concepts for solid oxide fuel cells (SOFCs) in stationary and mobile applications", Journal of Power Sources, vol. 127, pp.273-283, 2004.

[8] Weber et Al., "Oxidation of H2, CO, and methane in SOFCs with Ni/YSZ-cermet anodes", Solid State Ionics, vol.152-153, pp.543-550,2004.

[9] U. Stimming et Al., "Operation of anode-supported thin electrolyte film solid oxide fuel cells at 800 ° C and below", J. of Power Souces, V.71, pp.302-305, 1996.

[10] U. Stimming et Al., "Advances, aging mechanisms and lifetime in solid oxide fuel cells", J. of Power Souces, V.127, pp.284-293 , 2004.

[11] M. Mogensen et Al., "Durability and thermal cycling of Ni/YSZ cermet anodes for solid oxide fuel cells", Journal of Applied Electrochemistry, vol. 30, Issue 2, pp 247-257, 2000.

[12] T. Fukuia et Al., "Performance and stability of SOFC anode fabricated from NiO/YSZ composite particles", Journal of the European Ceramic Society, V. 23, pp. 2963–2967, 2003.

[13] T. Iwata et Al., "Characterization of Ni-YSZ anode degradation for substrate-Type solid oxide fuel cells", J. Electrochemical society, V.143, pp.1521-1525, 1996;

[14] Stover et Al., "Modelling of the agglomeration of Ni-particles in anodes of solid oxide fuel cells", V.36, pp.147-151,2001.

[15] Ioselevich et Al., "Degradation of solid oxide fuel cell anode", J. Electrochemical society, V.144, pp.3010-3018, 1997.

[16] C.C. Appel,"Durability test of SOFC cathodes", Journal of Applied Electrochemistry, V.30, pp.411-418, 2000.

[17] U. Stimming et Al., "Catalysis of the electrochemical processes on solid oxide fuel cell cathodes", J. of Power Souces, V.61, pp.205-211, 1998.

[18] Y. Nigara et Al., "Hydrogen permeability of YSZ single crystals at high temperatures", Solid State Ionics, V.171, pp.61-67 , 2004.

[19] M. Mogensen et Al., "Factors controlling the oxide ion conductivity of fluorite and perovskite structured oxides", ", Solid State Ionics, vol.174, pp.279-286,2004.

[20] F. Iguchi et Al., "Oxygen partial pressure dependence of creep on yttria-doped ceria ceramics", Solid State Ionics V. 176, pp. 641–644, 2005.

[21] G. Di Giuseppe et Al., "Fuel sensitivity tests in tubular solid oxide fuel cells", J. of Power Souces, V.125, pp.183-188 , 2004.

[22] Lee J.-H., Heo J.-W., Lee D.-S., Kim J., Kim G.-H., Lee H.-W., Song H.S., "Moon J.-H., The impact of anode microstructure on the power generating characteristics of SOFC", Solid State Ionics, vol. 158, pp. 225-232, 2003.

[23] Chan S.H., Khor K.A., Xia Z.T., "A complete polarization model of a solid oxide fuel cell and its sensitivity to the change of cell component thickness", Journal of Power Sources, vol. 93, pp. 130-140, 2001.

[24] A.VOL. Virkar, J. Chen, C.W. Tanner, J.W. Kim, "The role of electrode microstructure on activation and concentration polarizations in solid oxide fuel cells", Solid State Ionics, vol. 131, pp. 189-198, 2000.

[25] Lehnert W., Meusinger J., Thom F., "Modelling of gas transport phenomena in SOFC anodes", Journal of Power Sources, vol.87, pp. 57-63, 2000.

[26] T. Nishino, H. Komori, H. Iwai, K. Suzuki, "Development of a comprehensive numerical model for analyzing a tubular-type indirect internal reforming SOFC", proceedings of First International Conference on Fuel Cell Science, Engineering and Technology, Rochester NY, 2003.

[27] W.A. Rogers, R.S. Gemmen, C. Johnson, M. Prinkey, M. Shahnam, "Validation and application of a CFD-based model for solid oxide fuel cells and stacks", proceedings of First International Conference on Fuel Cell Science, Engineering and Technology, Rochester NY, 2003.

[28] P.W. Li, M.K. Chyu, "Simulation of the chemical/electrochemical reactions and heat/mass transfer for a tubular SOFC in a stack", Journal of Power Sources, vol. 124, n. 2, pp. 487-498, 2003.

[29] Bessette II N.F., Wepfer W.J., Winnick J., "A mathematical model of a solid oxide fuel cell", Journal of the Electrochemical Society, vol. 142, pp. 3792-3800, 1995.

[30] D. Arnost, P. Schneider, "Dynamic transport of multicomponent mixtures of gases in porous solids", Chemical Engineering Journal, vol. 57, pp. 91–99, 1995.

[31] P. Asinari, M. Coppo, 2004, "Influence of Porous Electrode Structure on PEM Fuel Cells Design and Performance", Proceedings of the 2nd International Conference on Fuel Cell Science, Engineering and Technology, ASME, Rochester N.Y..

[32] D. H. Rothman, 1988, Geophysics, Vol. 53, p. 509.

[33] J. Bernsdorf, M. Schafer, F. Durst, 1999, International Journal of Numerical Methods in Fluids, Vol. 29, p. 251.

[34] J. Bernsdorf, G. Brenner, F. Durst, 2000, "Numerical analysis of the pressure drop in porous media flow with

lattice Boltzmann (BGK) automata“, Computer Physics Communications, Vol. 129, p. 246-255.
[35] S. Succi, R. Benzi, F. Higuera, 1991, “The lattice-Boltzmann equation: a new tool for computational fluid dynamics”, Lattice Gas Methods: Theory, Applications and Hardware, edited by G. Doolen (Elsevier, Amsterdam), reprinted from Physica D, Vol. 47, p. 219.
[36] S. Chen, G. D. Doolen, 1998, “Lattice Boltzmann method for fluid flow”, Annual Review of Fluid Mechanics, Vol. 30, p. 329-338.
[37] Manz, L.F. Gladden, P.B. Warren, 1999, AIChE. Journal, Vol. 45, pp. 1845.
[38] Th. Zeiser, P. Lammers, E. Klemm, Y.W. Li, J. Bernsdorf, G. Brenner, 2001, Chemical Engineering Science, Vol. 56, pp. 1697.
[39] E.G. Flekkoy, 1993, Physics Review E, Vol. 47, pp. 4247.
[40] X. Shan, G. Doolen, 1995, Journal of Statistical Physics, Vol. 81, pp. 379.
[41] V. Sofonea, R.F. Sekerka, 2001, Physica A, Vol. 299, pp. 494.
[42] Z. Guo, T.S. Zhao, 2003, Physics Review E, Vol. 68, N. 035302.
[43] L.-S. Luo, S.S. Girimaji, 2003, Physics Review E, Vol. 67, N. 036302.
[44] K. Xu, 1997, Journal of Computational Physics, Vol. 134, pp. 122.
[45] K. Xu, 2000, Journal of Computational Physics, Vol. 163, pp. 349.
[46] P. Asinari, “Viscous coupling based lattice Boltzmann model for binary mixtures”, Physics of Fluids, 17, 067102, 2005.
[47] P. Asinari, M. Coppo, M.R. von Spakovsky, B.V. Kasula, “Numerical simulations of gaseous mixture flow in porous electrodes for PEM fuel cells by the lattice Boltzmann method”, proceedings of the “Third International Conference on Fuel Cell Science, Engineering and Technology”, Ypsilanti, Michigan, 2005.
[48] P. Asinari, “Asymptotic analysis of multiple-relaxation-time lattice Boltzmann schemes for mixture modeling”, International Journal Modern Physics C, 2005 (in press).
[49] P. Asinari, “Semi-implicit-linearized Multiple-relaxation-time formulation of Lattice Boltzmann Schemes for Mixture Modeling”, submitted to Physical Review E, 2005.
[50] V. Schulz, D. Kehrwald, A. Wiegmann, K. Steiner, “Flow, heat conductivity, and gas diffusion in partly saturated microstructures”, NAFEMS Simulation of Complex Flows (CFD), 2005.
[51] K. Schladitz, S. Peters, D. Reinel-Bitzer, A. Wiegmann, J. Ohser, “Design of acoustic trim based on geometric modeling and flow simulation for non-woven”, Berichte des Fraunhofer ITWM, N. 72, 2005.
[52] H. Okabea, M.J. Blunt, “Pore space reconstruction using multiple-point statistics”, Journal of Petroleum Science and Engineering, N. 46, p. 121– 137, 2005.
[53] J. Divisek, Y. Volfkovich and R. Wilkenhoener, J. Appl. Electrochem 29 (1999), 153-163.
[54] J.H. Ferziger, H.G. Kaper, 1972, “Mathematical Theory of Transport Processes in Gases”, North-Holland, Amsterdam.
[55] S. Chapman, T.G. Cowling, 1970, “The Mathematical Theory of Non-Uniform Gases”, Cambridge University Press, Cambridge.
[56] S. Harris, 1971, “An Introduction to the Theory of the Boltzmann Equation”, Holt, Rinehart and Winston, New York.
[57] B.B. Hamel, 1963, Ph.D. dissertation, Princeton University.
[58] B.B. Hamel, 1965, Physics of Fluids, Vol. 8, pp. 418.
[59] B.B. Hamel, 1966, Physics of Fluids, Vol. 9, pp. 12.
[60] G&K.
[61] Cercignani, 1975, “Theory and applications of the Boltzmann equation”, Scottish Academic Press, Edinburgh and London, UK.
[62] T. Abe, 1997, “Derivation of the lattice Boltzmann method by means of the discrete ordinate method for the Boltzmann equation”, Journal of Computational Physics, Vol. 131, p. 241.
[63] Y. H. Qian, D. D’Humieres, P. Lallemand, 1992, “Lattice BGK Models for Navier-Stokes Equations”, Europhysics Letters, Vol. 17, p. 479-484.
[64] Sone.
[65] N. MacDonald, E. Minty, T. Harding, S. Brown, “Writing Message-Passing Parallel Programs with MPI”, Edinburgh Parallel Computing Centre, The University of Edinburgh.
[66] R. Suwanwarangkul, E. Croiset, M.W. Fowler, P.L. Douglas, E. Entchev, M.A. Douglas, “Performance comparison of Fick’s, dusty-gas and Stefan–Maxwell models to predict the concentration overpotential of a SOFC anode”, Journal of Power Sources, vol. 122, pp. 9–18, 2003.
[67] R.C. Reid, “The properties of gases and liquids”, McGraw-Hill, New York, 1987.
[68] Larminie, J. and Dicks, A., 2000, “Fuel Cell Systems Explained” John Wiley and Sons Ltd., ISBN 0-471-49026-1.